Available online at www.sciencedirect.com

ScienceDirect

Procedia CIRP 22 (2014) 243 – 248

www.elsevier.com/locate/procedia

3rd International Conference on Through-life Engineering Services
Session: Recent Progress in Jet-Engine Regeneration

Multiscale Optical Inspection Systems for the Regeneration of Complex Capital Goods

Jochen Schlobohm*, Yinan Li, Andreas Pösch, Benjamin Langmann, Markus Kästner, Eduard Reithmeier

Institute of Measurement and Automatic Control, Leibniz Universität Hannover, Nienburger Straße 17, 30167 Hannover, Germany

* Corresponding author. tel.: +49-511-762-3236 ; fax: +49-511-762-3234. *E-mail address:* jochen.schlobohm@imr.uni-hannover.de

Abstract

The inspection of capital goods with complex geometries is a challenging task due to the limited maneuvering and measuring space available. We developed a set of optical measurement systems for the inline inspection of such machines and capital goods. At first we introduce a borescopic fringe projection system based on of-the-shelf components. It is capable of detecting geometric variances in hard to reach areas, e.g. inside machines or in between parts with highly complex geometries like blade integrated discs (blisks). Single parts like compressor blades are measured with an inverse fringe projection system, which uses fully adaptable fringe patterns. The adaptable patterns lead to a high sensitivity and high speed. Results can be achieved with only one fringe pattern per measurement.
In order to perform microscopic measurements and surface characterizations, we use a michelson interferometer with advanced 3D reconstruction algorithms to detect microscopic variances of the objects surface. These newly developed algorithms lead to higher sensitivity and improved results.
Together these three inspection systems enable us to detect and to quantify geometric defects or variances of different industrial parts. Based on this information the prediction of the reliability of a part can be improved and the lifetime of an industrial part can be extended leading to a reduction of maintenance costs.

Peer-review under responsibility of the Programme Chair of the 3rd InternationalThrough-life Engineering Conference

Keywords: metrology; inline measurement; mulstiscale; fringe proejction; borescope; white light interferometer; michelson interferometer;

1. Multiscale metrology in product regeneration

With the growing complexity of machines and their parts, determining their reliability is getting more and more complex. Additionally, higher integration of each parts functionality leads to a higher per part investment. Regenerating a part is therefore often more lucrative than replacing it. A central task in regenerating parts is determining their reliability. In order to give information about the reliability, complete, fast and precise measurements of the geometry of the part have to be carried out. Figure 1 shows an example of a very complex and hard to measure geometry. Optical measurement systems provide fast, precise data with high point densities [1]. State of the art tactile measurement systems have lower lateral resolutions and a lower measurement speed. They are designed for geometric inspection but are usually, due to the lower resolution, not capable of the detection of stochastic surface defects. Some parts are sensitive to contact so that they cannot be measured with tactile means. Therefore this paper concentrates on optical measurement systems. NovaCam [2] uses a rigid borescopic interferometer to scan the surface of an object point by point with very high precision (about 1 µm). Another approach by Storz [3] is triangulating 52 laser points with a videoscope. Classic fringe projection has the lack of needing multiple patterns projected on the object [4]. Most fringe projection systems are not capable of operating in very limited space as well. This paper introduces a borescopic fringe projection system as well as a ray tracing-based inverse fringe projection system.

The microtopography of turbine blades has an important impact on the functionality and efficiency of turbo machines because its aerodynamic boundary layer can determine the coefficient of skin friction. A surface of a blade at low Reynolds numbers has a laminar boundary layer, which causes a low skin friction [5]. The microtopography or surface roughness of turbine blade is usually measured with a confocal laser

Peer-review under responsibility of the Programme Chair of the 3rd InternationalThrough-life Engineering Conference
doi:10.1016/j.procir.2014.07.019

Fig. 1. A compressor blisk on display at the Paris Air Show 2013. This is a single-piece item, generated with 3D CNC milling. Source: Olivier Cleynen

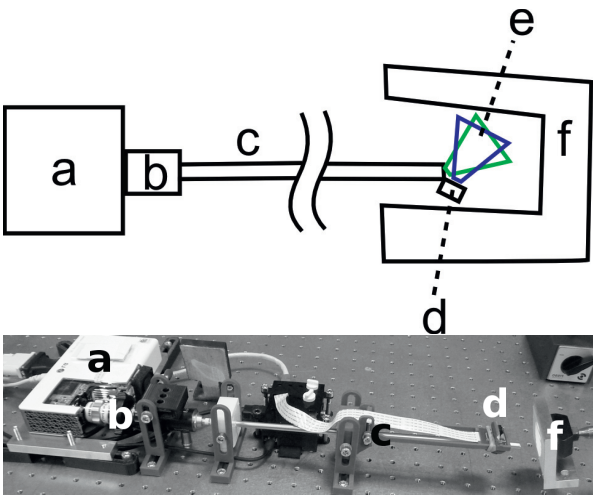

Fig. 2. Top: a) projector; b) borescope optics; c) borescope shaft; d) camera; e) fields of view; f) object. Bottom: borescopic fringe projection system with the projector (left), the borescope (middle) and the measurement head including the camera (right).

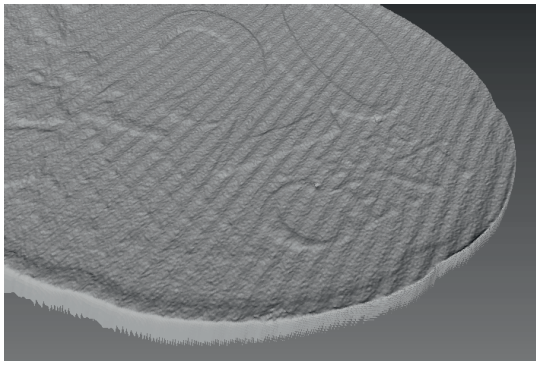

Fig. 3. Measurement with the endoscopic fringe projection system

scanning microscope (CLSM) or with a white light interferometer (WLI). In order to produce data of higher quality, a roughness measurement using WLI is generally more suitable. The scanning accuracy and time of a WLI or CLSM depend on the type of algorithm used for the reconstruction of the 3D surface shape as well as the hardware performance. The working principle and the differences between the measurement system are presented in detail in [6]. In this paper we present a space-saving construction of low-coherence Michelson interferometer [7] determination, which can perform precise nanoscale spatial measurements in the small space between two blades and reach areas unsuitable for common interferometers due to their geometric dimensions, e.g. a Mirau interferometer or a Linnik interferometer.

2. Advanced fringe projection systems

2.1. Inline measurements with a rigid borescopic fringe projection system

This work introduces a newly developed rigid borescopic fringe projection system. The need of geometry inspection in between parts of complex geometries led to the development of a fringe projection system with a very small measurement head (see figure 2). Our prototype was partly build from consumer electronics: a portable LED-beamer and a raspberry pi single-board computer along with a mobile phone 5 mega pixel camera. But we are also using a professional rigid boresope from *Storz* for the projection of the measurement patterns. The combination of a borescope with the principle of a videoscope leads to a compact and low-cost measurement system with optics needed for the projection of fringe patterns inside complex geometries.

With the borescope we are able to take advantage of the very cost efficient projector and its high resolution and high contrast projections while the system is non the less capable of measuring in very limited spaces. It is for example capable of scanning areas in between two blades of a blisk (see figure 1), where a classic fringe projection system has problems with areas covered by a neighboring blade. When measuring complex geometries, classic fringe projection systems usually lack of precision because of a large angle between the line of sight and the surface normal. The borescopic fringe projection system can reach into a complex object to be aligned in an optimal angle to improve the results. Using state of the art camera calibration as shown in [8], influences caused by mediocre lens and camera quality can be minimized. Based on this technique Pösch et al. [9] developed algorithms for the calibration of stereoscopic systems consisting of a camera and a projector.

Figure 3 shows a measurement of a 20 euro cent coin. The

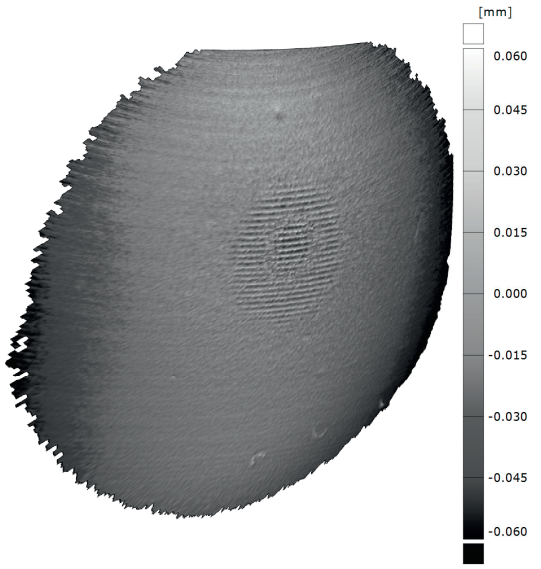

Fig. 4. Measurement of a high precision ball (diameter: 30mm)

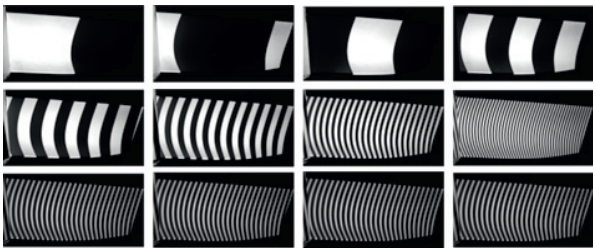

Fig. 5. Fringe projection patterns for phase unwrapping of a compressor blade.

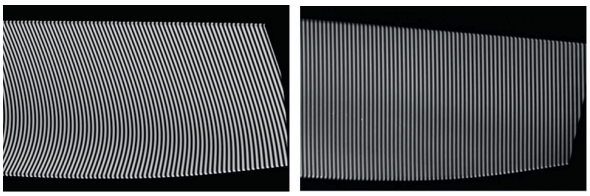

Fig. 6. Inverse fringe patterns of a turbine blade. Left: Inverse fringe pattern of the projector. Right: camera image of inverse fringe pattern without geometry defects.

whole coin consists of 1.1 million data points. The field of measurement is 30×30 mm^2 with the coin having a radius of approximately 25 mm. The surface of the coin seems to be bend although the real coin is mostly planar. Using multiple lens systems for projecting the images leads to a complex distortion of the projected images. The distortion model we are using seems to be insufficient to minimize those effects adequately. Additionally, one can see regular ripples in the measurement data. Those ripples are a result of an insufficient gamma-correction. Psychovisual optimization done by the projector and camera lead to a nonlinear gamma curve. We implemented a gamma correction based on a power-law function [10] which is not able to compensate those effects.
On the other hand one can see that the measurement resembles the coins geometry very well. Even small features, like the outline of Italy in the map of Europe, are preserved. Figure 4 shows an uncertainty map of a measurement of a ball with a 30 mm diameter. Most of the data points have an uncertainty of approximately 30 µm. The system is still an early prototype, the estimation of measurement uncertainties is still subject to research.

2.2. High speed and high sensitivity geometry measurements

In addition we have developed a macroscopic fringe projection system. The system consists of a consumer high definition projector and an industrial camera. It can measure objects that fit in a 140 mm x 100 mm x 50 mm box. Compared to the earlier described endoscopic system, the measurable volume is bigger and the lateral resolution smaller. We use this system for the measurement of hand sized objects like turbine blades and for the development of inverse fringe projection.
In classic fringe projection there is a projector and a camera setup in a known triangulation angle as described in [4]. Patterns with straight and equidistant lines are projected onto the object. The geometry is then calculated from the distorted lines the camera detects. One disadvantage of this technique is that multiple projection patterns are needed to identify the projected lines (see figure 5). Otherwise disambiguation is not guaranteed. Even Tsang's method for structured light 3D measurements [11] needs at least three projected patterns.
Our approach is projecting patterns which lead to straight and equidistant lines in the camera image. This is achieved by a ray tracing simulation of the measurement scene, where the camera and the projector are exchanged [9]. The virtual projector then projects lines onto the object. The rendered virtual camera image is afterwards used with the real projector. If the object has no geometric variances, the real camera will detect straight and equidistant lines (see figure 6). Geometrical defects lead to distorted lines in the camera image (see figure 7). Analysis of those images leads to the detection and approximate quantification of variances. The Hilbert transform [12] is used to compute variances in the images sinus like waves phase. The transform is similar to fitting such waves into the image, which has also a similar affect as applying a noise filter. Variances can be detected using only one image. If a defect is found, precise quantification may be done with classic fringe projection or any other measurement system. In order to render the simulation the objects nominal geometry as well as its location and orientation have to be known. Therefore this technique is applicable in a regeneration process: The geometry and pose of the object are determined at the beginning of the regeneration process. The object itself is clamped in a zero-point clamping system, so that the pose remains the same even if the object has been removed for processing. Inverse fringe projection then detects geometric variances in between regeneration steps (e.g. welding, soldering, milling). Another approach for fast pose estimation is discussed in [13]. Inverse fringe projection is implemented in software, so it can be used with existing fringe projection systems with pixel based projection.

Figure 8 shows the rendered point cloud of a measurement of the same 20 euro cent coin shown in figure 3, measured with

Fig. 7. Camera image of inverse fringe projection with a defect geometry.

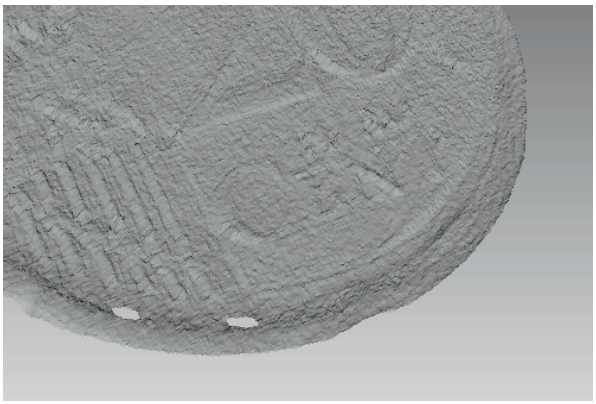

Fig. 8. Rendered measurement of a 20 euro cent coin. Measurement taken with macroscopic fringe projection system.

classic fringe projection patterns. The dataset consist of approximately 115000 data points. The field of measurement is $140 \times 95 mm^2$ with the coin in the center of that area. The standard deviation of the uncertainty is approximately 20 µm.

3. Microstructure measurement system

3.1. Configuration of a low-coherence Michelson Interferometer (LCI)

In order to meet the requirements of low measurement uncertainties and to shrink the sensor volume for the special need of the geometries of blisks or turbine blades, an interferometer is constructed using the principle of the low-coherence Michelson interferometer (see figure 9). Figure 10 shows the schematic optical design of the interferometer. It consists of four modules, a polarizer beam splitter, a Köhler-illumination [14] with a low-coherence deep red light-emitting diode (LED) as light source, a charge coupled device (CCD) camera with telecentric lens and a reference mirror with a rotatable polarizer on a linear nanopositioning stage. The spatially homogeneous LED light from the Köhler-illumination system is divided by the beam splitter into two perpendicular 50% transmitted beams, a measuring beam and a reference beam. They have the same length of optical path and project on the surface of the measuring probe and on a reference mirror separatively. Their

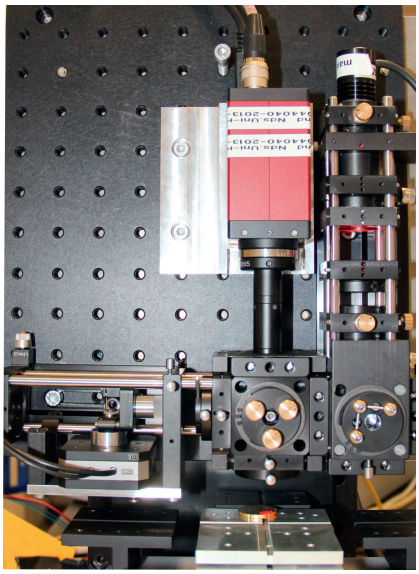

Fig. 9. a prototype of the low-coherence Michelson interferometer

reflected beams are routed by the beam splitter towards the CCD-camera and superposed, thus, an interferogram can be obtained by the CCD-camera. Both beams may have different intensities, one created by diffuse reflection, the other by specular reflection, which leads to low contrast. Therefore, the intensity of the specular reflected light can be manual adjusted with the rotation angle of the rotatable polarizer to get a high contrast interferogram.

In the surface measurement procedure, the reference mirror is moved parallel to the reference beam with a scan step width, which is considerably shorter than the wavelength of the light source. In order to improve the motion accuracy of the nanopositioning stage, the movement controller uses a single-axis driver with a closed-loop mode. With every move of the reference mirror, the CCD-camera will record the interference pattern referenced to the z-position in a data stack (see figure 11). To shorten the synchronization between the mirror movement and the interferogram recording, an Arduino microcontroller is used, which with the sampling time for a scan step was improved to 150 ms. The movement distance of the reference mirror, i.e. the scan length, depends on the maximum height difference or roughness of the test surface.

As the reference mirror moves, the recorded interferograms change with the length difference of the reference arm. A data stack stores all the interferograms in a layered structure. Each of the pixels on the interferogram in z direction corresponds to a signal, which is a continuous intensity variation changing with different length of the reference arm. Before the signal analysis, every signal is filtered by a second order band-pass filter. By calculating the maximum intensity of the envelope of scanned data stack in z direction, the relative surface height can be obtained. Figure 11 indicates the detection of the maximum amplitude position of a signal by the Hilbert Huang Transform [15]. According to the roughness of the test surface, the interferometric test bench in this paper uses a scan step

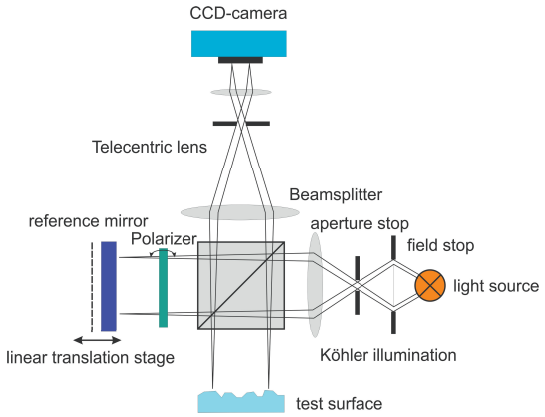

Fig. 10. Setup of a low-coherence Michelson interferometer

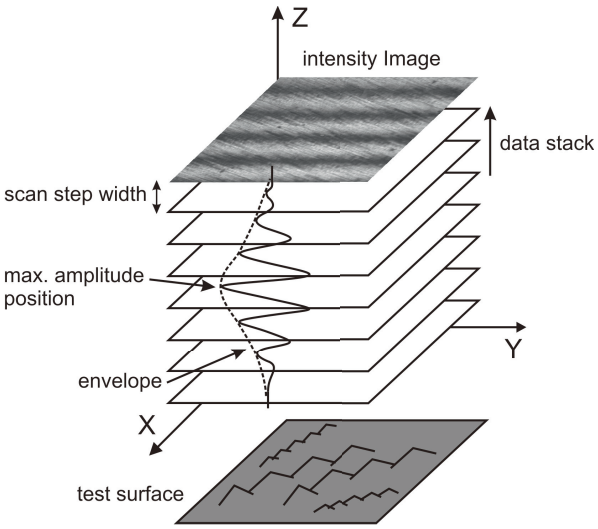

Fig. 11. Signal processing of a interferogram stack using the envelope detection

with 50 nm and a deep red light-emitting diode (LED), which has a 640 nm peak wavelength. After scale calibration with a calibration artifact, the vertical resolution of this interferometer can reach to 10 nm.

3.2. *Experimental results of the interferometer*

In order to obtain the accuracy and applicability of the proposed low-coherence interferometer, the same 20 euro cent coin, which was used in section, was measured in this case. To get a high lateral resolution, we use a telecentric lens with 4 x magnification and set the CCD-camera with a resolution of 2452 pixels x 2054 pixels and 8 bit per pixel. The lateral resolution of the system was calibrated using a silicon resolution standard (SiMETRICS Type RS-M) with 20 µm pitch value. In this experimental setup, the lateral Measurement Range was closed to 1.8 x 2.1 mm^2. Before the measuring, the rotation angle of the rotatable polarizer is adjusted, depending on the reflected light intensity of the metal surface, to optimize the contrast of the interferogram.

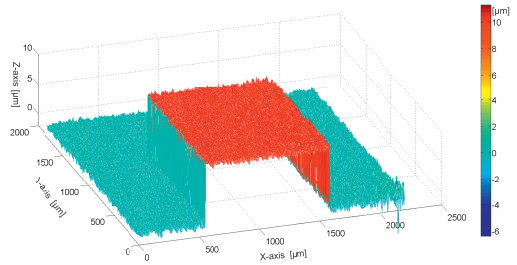

Fig. 12. Checking the vertical and lateral accuracy and resolution with a 9.908 µm step height standard

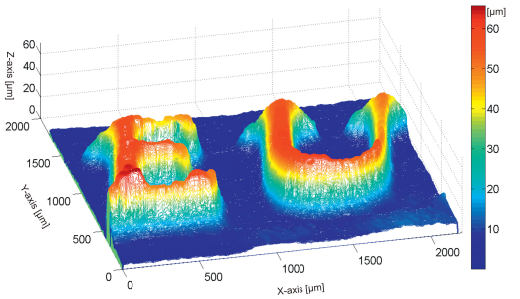

Fig. 13. 3D plot of a part of 20 euro cent

To check the vertical and lateral accuracy and resolution, a step height standard of Veeco with a 9.908 µm height and an approx. 1000 µm width was measured by our interferometer. The results are shown in figure 12, where the measured step has an average height of 9.956 µm and an average width of 1017 µm. The measurement accuracy can be limited by mechanical imperfections of motion control components, thermal drift and acoustic vibrations. Although there are some limits, the vertical resolution can be improved with factors such as a smaller scan step of the linear translation stage and a lower slope of the object surface regarding the optical axis of the telecentric lens.

Figure 13 shows a 3D plot of small piece of metal surface on the lower part of the 20 euro cent coin. The two letters EU above the surface have an approximate average height of 55 µm. Some coarse or irregular surfaces of the coin have non reflective surfaces like a scratch or pit on the surface, which cannot reflect the rays to CCD-camera,so that some camera pixels are located at dark regions during the measurement. Therefore, the pixels in these regions have no available information to calculation height values. These pixels are approximated with the help of a 2D median filter, bandwidth filter, etc [16]. The scanned 3D surface data in figure 13 is filtered with a 2D Gaussian filter. Also, our program uses different filtering algorithms for different regions according to characteristics of the material surface or height distribution.

The surface property of worn turbine blades can be determined with the use of a LCI. Figure 14 shows the leading edge of a real scanned surface of such a worn turbine blade after the removed of the protective layer. The leading edge of the blade

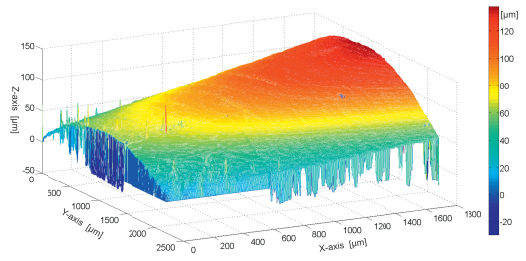

Fig. 14. 3D plot of a scanned surface on the leading edge of a worn turbine blade without protective layer

usually becomes damaged. Therefore, the scanned surface of a real-life turbine blade in figure 14 shows defects, such as an approx. 20 µm dent at the top, a few small nicks in the middle and some unmeasured pits on the convex sides. Those pits remain unmeasured because they do not hold any available height information due to the lack of reflected light. The great curvature of the leading edge causes a lot of the LCI light source to be deflected. At the same time much of the ambient light is reflected into the LCI, so that the measured surface of the convex sides contain a lot of noise and irregularities.

4. Conclusions

With the three measurement systems presented in the paper we are capable of performing multiscale geometric inspections of complex parts. While the endoscopic fringe projection system is designed for in-line inspection having a very small measurement probe, the macroscopic fringe projection system implements advanced algorithms for fringe projection and is able to inspect one blade with a single measurement. The next step is to improve the measurement quality of the borescopic system, implementing improved models for lens distortion and gamma-correction. Moreover, we are going to use inverse patterns for both fringe projection systems. Future research will take bending of the borescope due to gravity into account.

The current prototype of the low-coherence Michelson interferometer allows precise quantitative measurements with the resolution of 10 nm in vertical direction and 10 µm in lateral direction. Surface regions with very low light-reflection that are located at areas with high curvatures cannot provide any available information to evaluate the height information. In addition, thermal drift and acoustic vibrations can affect the measurement accuracy. In the next step we will develop effective algorithms to minimize the effects of drift and a parallel computing architecture to evaluate height information of large amounts of data for less computation time.

Acknowledgements

We would like to thank the German Research Foundation (DFG) for funding this project within the Collaborate Research Center (SFB) 871 ”regeneration of complex capital goods” (http://www.sfb871.de).

References

[1] Koch, A.. Optische Messtechnik an technischen Oberflächen. Expert-Verlag; 1998. ISBN 9783816913726.
[2] NovaCam, . Profilometers: Microcam. NovaCam; 2014. URL: http://www.novacam.com/products/profilometers/.
[3] Storz, . Messsysteme und Dokumentation. Storz; 2014. URL: https://www.karlstorz.com/cps/rde/xchg/karlstorz-en/hs.xsl/15522.htm.
[4] Kästner, M.. Optische Geometrieüberprüfung präzisionsgeschmiedeter Hochleistungsbauteile. Ph.D. thesis; Leibniz Universität Hannover; 2008.
[5] Ren, J., Sundararajan, S.. Nanoscale surface roughness affects low reynolds number flow: Experiments and modeling. Micro/nano scale surface roughness tailoring and its effect on microfluidic flow 2013;:P.100.
[6] McGeouch-Flaherty, C.A.. Proton assisted dissolution of the dental hard tissue enamel as a non-bacterial process. Ph.D. thesis; University of Warwick; 2011.
[7] Michelson, A.A., Guillaume, C.E.. Détermination expérimentale de la valeur du mètre en longueurs d’ondes lumineuses. Gauthier-Villars et fils 1894;.
[8] Zhang, Z.. A flexible new technique for camera calibration. IEEE Transactions on Pattern Analysis and Machine Intelligence 2000;22(11):1330–1334.
[9] Pösch, A., Vynnyk, T., Reithmeier, E.. Fast detection of geometry defects on free form surfaces using inverse fringe projection. Journal of the CMSC 2013;8(1):10–13.
[10] Hoang, T., Pan, B., Nguyen, D., Wang, Z.. Generic gamma correction for accuracy enhancement in fringe-projection profilometry. Opt Lett 2010;35(12):1992–1994. URL: http://ol.osa.org/abstract.cfm?URI=ol-35-12-1992. doi:10.1364/OL.35.001992.
[11] Zhang, S., Yau, S.T.. High-resolution, real-time 3d absolute coordinate measurement based on a phase-shifting method. Opt Express 2006;14(7):2644–2649. URL: http://www.opticsexpress.org/abstract.cfm?URI=oe-14-7-2644. doi:10.1364/OE.14.002644.
[12] Oppenheim, A.V., Schafer, R.W.. Zeitdiskrete Signalverarbeitung. Oldenbourg; 1995.
[13] Schlobohm, J.. Poseschätzung von Freiformobjekten anhand von Kontur- und projizierten Merkmalen in der Messtechnik. Master’s thesis; Leibniz Universität Hannover, Institut für Informationsverarbeitung (TNT) and Institut für Mess- und Regelungstechnik (IMR); 2013.
[14] Köhler, A.. Ein neues Beleuchtungsverfahren für mikrophotographische Zwecke. Zeitschrift für wissenschaftliche Mikroskopie und für mikroskopische Technik 1893;10:433–440.
[15] Huang, N.E., Shen, S.S.. Hilbert-Huang transform and its applications. World Scientific; 2005.
[16] de Groot, P., Colonna de Lega, X., Kramer, J., Turzhitsky, M.. Determination of fringe order in white-light interference microscopy. Applied optics 2002;41:4571–4578.